Materials and Design 32 (2011) 3421–3430

Contents lists available at ScienceDirect

Materials and Design

journal homepage: www.elsevier.com/locate/matdes

Process parameter influence on performance of friction taper stud welds in AISI 4140 steel

D.G. Hattingh [a], D.L.H. Bulbring [a], A. Els-Botes [a,*], M.N. James [a,b]

[a] Friction Processing Research Institute, Faculty of Engineering, The Built Environment & Information Technology, Nelson Mandela Metropolitan University, Port Elizabeth 6031, South Africa
[b] School of Marine Science & Engineering, University of Plymouth, Drake Circus, Plymouth PL4 8AA, UK

ARTICLE INFO

Article history:
Received 25 June 2010
Accepted 1 February 2011
Available online 26 February 2011

Keywords:
D. Welding
A. Ferrous metals and alloys
E. Mechanical

ABSTRACT

Friction taper stud welding is a new variant of friction welding which has been developed from the principles of friction hydro-pillar processing. This paper considers the effect of weld process parameters on weld defects, macrostructure and mechanical properties in AISI 4140 steel. It also presents 3D residual stress data for a typical friction taper stud weld. Applied downwards force, rotational speed and plunge depth (equivalent to consumable length) of the stud tool were systematically varied whilst measuring tool torque and temperature at several locations during welding. A simple Taguchi analysis was then used to relate process parameters and weld tensile strength. The combinations of parameters leading to high tensile strength are identified and linked to the occurrence of specific weld defects.

1. Introduction

Friction taper stud welding (FTSW) is a newly developed solid-state process that could beneficially replace conventional fusion welding techniques in certain residual life assessment and repair procedures widely used in thermal power plant, e.g. for creep damage and localised cracking in thick-walled high pressure steam pipe of the types discussed in Ref. [1], or in repair of alloys that are hard to fusion weld. The maintenance of high temperature plant, together with assessment and management of their residual life, are important and expensive issues for the operators of power generation plant. One ongoing difficulty relates to the necessity of sampling creep damage through the thickness of thick-walled steam pipe. Early methods of creep damage assessment were based on visual non-destructive methods, e.g. surface replication, to measure void area ratios [1]. These techniques were extended into semi-destructive surface trepanning methods which allowed creep damage to be directly assessed but only in the outer part of the wall thickness of the pipe [2]. Such direct material sampling via a boat or scoop is used when detailed microstructural information on degradation is necessary to support life assessment or extension. When knowledge of degradation and creep damage is required throughout the thickness, it is common for a section of the pipe to be cut out and a new section to be welded in place. This is time consuming, expensive and requires plant shut-down. The obvious extension of this scoop process is into developing a combined coring/cavity filling weld repair process that allows assessment of creep damage through the majority of the wall thickness, and that is fast, efficient and cost-effective.

This concept of more thorough assessment and repair of localised damage led to the development of friction hydro-pillar processing (FHPP) [3,4] and friction taper stud welding (FTSW) [5] to accomplish coring and then cavity filling using a consumable tool. These techniques give less microstructural perturbation and lower residual stress levels than would occur with fusion welding. They also offer considerable time, energy and cost savings over fusion welding in this application.

FHPP was developed at TWI [4] for specialist localised damage repair applications such as underwater cracks and fixing blast furnace lining dowels to the inside of the vessel under hot conditions. Further work on the FHPP technique extended its potential applications to crack repair, hole filling, cladding and material processing [6]. As noted in Ref. [6], the FHPP technique involves rotating a consumable tool concentrically in a hole whilst applying a downwards load, to continuously generate a localised plasticised layer. The plasticised material develops at a rate faster than the axial feed rate of the consumable tool, and hence the frictional rubbing surface rises up along the length of the tool giving a dynamically recrystallised interface layer which forms the weld. Linear welds, suitable for repairing more extensive cracks, could be made via a series of overlapping stitch welds and the technique was also trialed underwater [7]. Ambroziak and Gul [3] reported further work on the use of the process for the repair of undersea structures, including oil pipelines. They considered S355 structural steel welded in a special tank simulating marine conditions. This steel is

* Corresponding author. Tel.: +27 41 504 3091; fax: +27 41 504 9422.
E-mail address: Annelize.els-botes@nmmu.ac.za (A. Els-Botes).

0261-3069/$ - see front matter © 2011 Elsevier Ltd. All rights reserved.
doi:10.1016/j.matdes.2011.02.001

widely used in the offshore construction, pipeline and marine industries and the authors found that welds of 'sufficient' quality could be produced only for stud diameters between 10 and 12 mm with a hole depth of 25 mm.

The FHPP technique is capable of producing very good quality welds, using a parallel hole geometry, in steel and certain non-ferrous materials, characterised by good impact, tensile and bend properties [8]. One issue noted particularly in welds made with parallel-sided holes, where a comparatively high rotational speed and a high consumable feed rate were used, was that sudden changes in microstructure were sometimes observed. These were considered to be the result of an almost instantaneous shift in the rotational frictional interface [8] caused by seizure of the rotating consumable tool at its current frictional interface and then shear at a location some distance further along the tool, leading to the creation of a new frictional interface. To ameliorate this problem, it was proposed [8] that tapered holes and consumables with a correspondingly more acute taper could be used. This enabled a reactive force as well as hydrodynamic force to be exploited in making the joint. This variant of the technique enabled FHPP welds to be made in materials otherwise regarded as difficult to extrude or flow at forging temperature. The authors in Ref. [8] also observed that the angle of the taper would be to some extent material-dependant, noting that included angles of less than 30° for certain copper alloys and angles of less than 25° for aluminium alloys would be preferred.

A comprehensive process-parameter-microstructure–property matrix was explored in the work of Pinheiro [9], which also gives an up-to-date summary of the available literature on FHPP. It observes that that only a limited number of groups are working on this process and that many publications have essentially the same content, making difficult a comprehensive literature review. It also noted that in FHPP the consumable tool and the bore hole can be of different geometries and shapes, including a tapered configuration. The welding consumable plasticises across the whole diameter and across the whole welding depth. Pinheiro [9] observes that alternate terms are also used to describe variants of the FHPP, e.g. friction taper plug welding describes friction welding processes where a through-thickness hole is closed by friction welding a rotational tool to the sidewall of the hole. The welding consumable is then only plasticised near the surfaces and not across the whole diameter. The GKSS work reported in Ref. [9] extended the use of tapered FHPP to creep-resistant and cost-effective die casting magnesium alloys. It considered the influence of two key experimental parameters, downwards welding pressure, which was considered the most influential welding parameter, and the rate of shortening of the tool. In their welds the included angle of the tool was 10° and that of the hole was 20°. Transverse tensile and pull-out testing confirmed the feasibility of the process to produce high strength welds, with failures taking place outside the welded area in most of the cases. In his final conclusions Pinheiro [9] noted that a wide operating window exists for FHPP of cast magnesium alloys for the production of good quality welds based on their mechanical properties.

Work by the present authors has focussed on repairing localised damage in thick walled steel components, where the damage is removed by coring out a tapered blind hole and then filling the hole with a rotating tapered consumable tool. They have termed this variant of FHPP friction taper stud welding (FTSW) [5,10]. The tool has a slightly smaller included angle than the hole into which it is inserted. Heat is generated by frictional rubbing between the two surfaces, which initially occurs at the bottom of the hole. The difference in angle between tool and hole allows plasticised material to move upwards along the tool/hole interface leading to progressive plasticisation of the total interface during plunging of the tool. The plunge depth of the tool, which is directly analogous to the length consumed during welding, has been previously termed "burn-off" by several authors [e.g. 3]. However, the carry-over of this term from arc welding into friction processing is inappropriate for a solid-state process where measured peak temperatures in welding of steel are around 1150 °C, compared with a melting temperature of around 1450 °C for low alloy steel. Plunge depth and pressure are important parameters in allowing plasticised material from the consumable tool to completely fill the gap between the tool and the hole, hence giving a sound solid-state weld. As noted below, one of the advantages of the FTSW process is that larger diameter studs can be used with a lower probability of lack-of-fusion defects at the stud–hole interface.

The seemingly minor variation of the inclusion of a taper in the FTSW process addresses a limitation in FHPP on the stud tool diameter and length that be used in successful welding [3] whilst retaining all the benefits of solid-state processing. These include fewer defects from the melting–solidification process, less microstructural perturbation and lower residual stress levels after welding. The process also lends itself to automation and thus increased process and quality control. Another advantage of FTSW arises from the ability conferred by the taper to prolong the duration of welding, compared with FHPP which means that increased temperatures can be attained. This allows a wider range of materials to be friction welded and forged by the FTSW method [6]. It would be anticipated that the included angles of the tapered tool and the hole in the workpiece would be of fundamental importance in FTSW. A significant amount of initial work was undertaken to establish a value for these included angles and their difference that would allow acceptable welds to be made with a larger diameter hole than reported for FHPP [3]. An included tool taper angle of 15° with an included hole angle of 20° was found to give satisfactory welds for a hole approximately 21 mm diameter by 16 mm deep and these values were used throughout this work.

In developing the FTSW process, work by Hattingh et al. [5] and Van Zyl [10] considered friction taper stud welding of creep-resistant chrome–molybdenum alloy steel (10 CrMo 9 10) used for high pressure, high temperature steam pipe in thermal power generation. The plain profile consumable tool was manufactured from the same alloy. Van Zyl [10] modelled the heat flow and temperature distribution but did not consider the effects of change in weld parameters on weld quality and performance.

The work reported in the present paper extends the technique to the higher strength AISI 4140 steel and considers the influences on weld integrity of process parameters such as the applied downward forging force on the tool, rotational speed and plunge depth (consumable length). 4140 is a 1% chrome–molybdenum medium-hardenability steel that is characterised by high strength and good impact properties, but low weldability. It is therefore a good candidate to demonstrate the utility of FTSW for repairing local damage.

2. Experimental procedure

Fig. 1a shows the purpose-built FTSW machine which is hydraulically operated while Fig. 1b shows a typical completed friction taper stud weld; the stud is then cut off and the excess material dressed back to provide a smooth surface on the block. Fig. 2a gives geometrical details of both the tapered consumable tool and the hole which is filled during the welding process. As noted above, the consumable tool has a 15° taper and the corresponding hole has a 20° taper. Table 1 gives the composition of the 4140 steel which was used to manufacture both the tool and the block to be welded.

In addition to the relative taper angles of the tool and hole, the parameters important to the integrity of FTSW have been identified as the downward force, rotational speed and plunge depth.

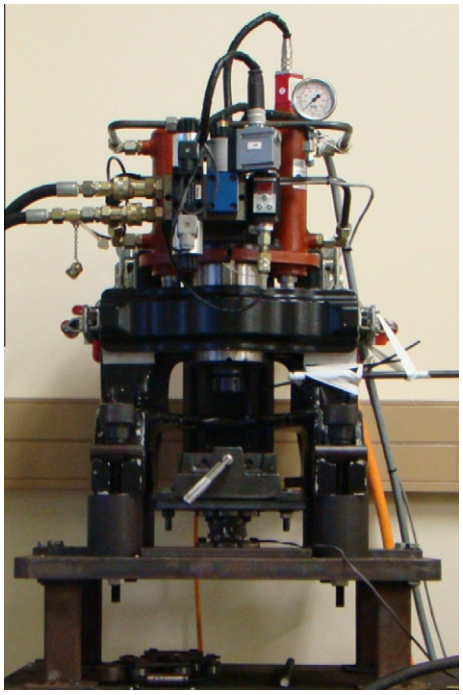

Fig. 1a. Friction taper stud weld setup.

Fig. 1b. Completed friction taper stud weld in 24 mm thick 4140 steel.

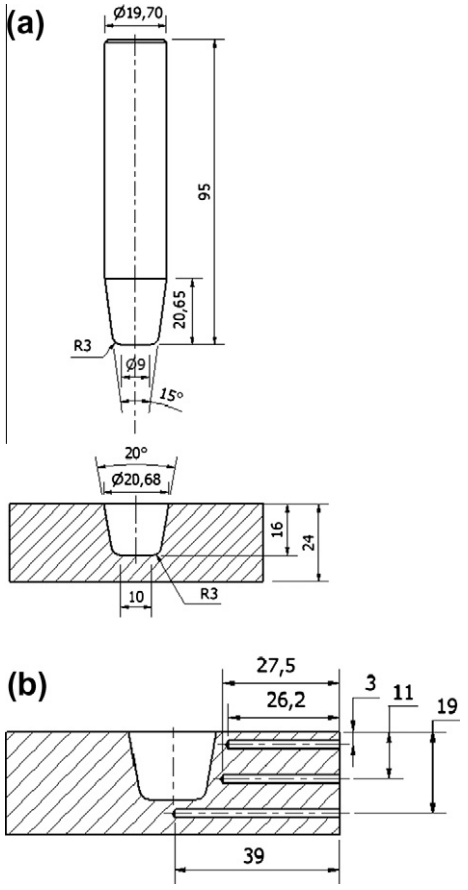

Fig. 2. (a) Dimensions of tapered consumable tool and tapered hole. (b) Position of thermocouples used to measure temperature.

Table 1
Standard chemical composition in wt.% and mechanical properties of AISI 4140 medium carbon steel.

Chemical composition	C	Si	Mn	Cr	Mo
Suppliers specifications	0.36–0.44	0.1–0.35	0.7–1	0.9–1.2	0.25–0.35
Measured values	0.41	0.338	0.85	1.04	0.217
Mechanical properties	Yield (MPa)	UTS (MPa)	Microhardness (HV 500 gf)		
Measured values	800	975	306		

In this prototype FTS welding machine the hydraulic control system was not precise enough to achieve set values of applied downward force or plunge depth. Initial work had indicated that the minimum tool plunge depth required to completely fill the hole was approximately 2.4 mm. A minimum plunge depth of 4 mm was then chosen to allow for machine control inaccuracies to provide sufficient plasticised material to ensure that sound welds were made. The maximum plunge depth was chosen to give a ratio of approximately 2.5 between the volume of material displaced from the tool during plunging and that of the original hole volume to be filled, which is defined as the residual hole volume with the stud in position at the start of the weld. An empirical approach was therefore adopted to identify ranges of input variables within the process window capabilities of the FTSW platform which experience had demonstrated gave similar weld 'quality'. Table 2 gives the values used in the 27 experimental test welds (marked P1 to P27) of the three weld process parameters of applied downward force, tool rotational speed and plunge depth (equivalent to consumable length), characterised into three platform-specific process bands of low (*L*), medium (*M*) or high (*H*). Plunge depths between 3 and 5 mm are considered as 'low (*L*)', between 5 and 7 mm as 'medium (*M*)' and between 7 and 9 mm as 'high (*H*)', whilst applied downward force values between 9 and 12 kN are termed 'low', between 20 and 22 kN are 'medium', and between 26 and 28 kN are 'high'. Temperature was measured throughout the welding process with thermocouples that were positioned at a distance about 3 mm from the original hole boundary and at depths below the surface of 3 mm, 11 mm and 19 mm. The tip of the thermocouple at the 19 mm depth coincided with the centreline of the hole (see Fig. 2b). Tool torque was also measured during welding.

Once the welds had been made, they were sectioned to allow characterisation of the microstructure and microhardness across the weld zone. Fig. 3 illustrates the matrix of microhardness

Table 2
Full experimental matrix of tool speed, downwards force and plunge depth values.

Test No.	Tool rotational speed (rpm)			Downwards applied force (kN)			Tool plunge depth (mm)			Vickers hardness (H_V)			Length of flash crack (mm)
	L	*M*	*H*	*L*	*M*	*H*	*L*	*M*	*H*	(0;3)	(12;3)	(0;15)	
P1			6000	10.5			4.5			621	642	606	2.3
P2			6000		20.6		4.0			570	589	529	3.5
P3			6000			27.5	3.2			650	624	650	4.3
P4			6000	10.9				6.3		575	423	568	0.8
P5			6000		20.6			6.5		629	631	624	3.2
P6			6000			27.1		5.4		606	682	531	5.5
P7			6000	11.7					9.0	369	452	347	0.7
P8			6000		20.6				7.9	523	552	759	2.8
P9			6000			27.5			7.7	656	626	703	3.8
P10		4250		9.3			4.1			510	453	830	–
P11		4250			21.0		4.1			719	577	788	1.7
P12		4250				27.5	4.0			752	752	784	2.5
P13		4250		10.5				5.7		599	495	589	–
P14		4250			20.2			5.8		650	584	805	1.3
P15		4250				26.7		5.2		709	706	826	2.8
P16		4250		11.3					9.0	387	458	406	–
P17		4250			21.0				7.9	603	546	532	4.4
P18		4250				27.9			7.6	606	563	515	5.6
P19	2500			10.9			4.5			599	606	673	0.9
P20	2500				21.4		4.0			712	642	631	2.6
P21	2500					27.9	3.0			276	272	645	6.9
P22	2500			10.9				6.6		647	682	570	–
P23	2500				21.0			6.6		557	568	670	2.6
P24	2500					26.7		6.3		601	528	642	2.5
P25	2500			10.5					8.2	510	482	454	2.1
P26	2500				21.0				8.5	566	648	629	1.7
P27	2500					26.7			7.3	670	632	653	2.2

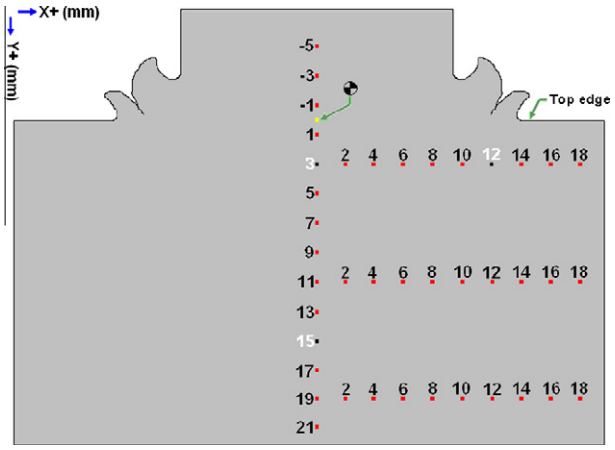

Fig. 3. Micro-hardness measurement positions; the numeric values are dimensions in millimetres in the x and y-directions.

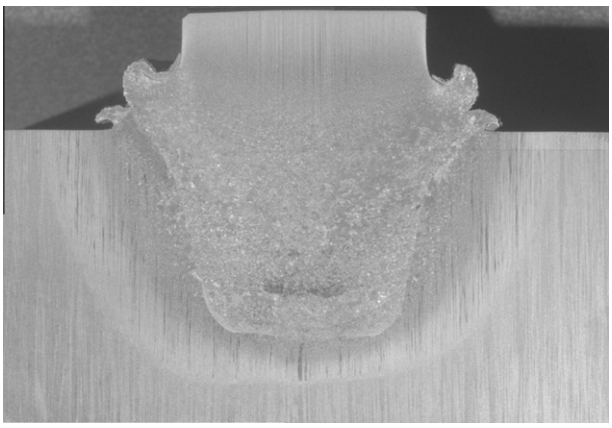

Fig. 5a. Weld macrograph of a typical friction taper stud weld.

measurement positions which were spaced at 2 mm intervals horizontally and vertically and are characterised by their (x, y) coordinates. The hardness measurements which are given in Table 2 are highlighted in Fig. 3 for positions $(x, y) = (0, 3)$, $(12, 3)$ and $(0, 15)$. Tensile tests [11] were performed on hourglass specimens (Fig. 4d) initially machined as 4 mm thick slices (Fig. 4c) sectioned from the centre of the weld (Fig. 4b) after removal of the remaining protruding stud, using water jet cutting. Tensile data are given in Table 3 and discussed in Section 3.3.

3. Results and discussion

3.1. Weld macrostructure and hardness

Etching the welds in a 2% nital solution revealed the weld macrostructure and a typical example of a FTS weld is shown in Fig. 5a. Close examination allows several distinct zones to be distinguished as indicated in the illustration given in Fig. 5b. For the purposes of the present discussion these are termed the forged zone (FZ), toolplate interfacial mixing zone (MZ), stir zone (SZ), high temperature heat affected zone (HT HAZ) and low temperature HAZ (LT HAZ).

Fig. 6 shows the characteristic 'flash' that is extruded at the tool–hole interface as a result of plasticisation of the hole wall and tool. The interface between these two streams of plastic material forms a sharp crack-like defect the details of which are clearly important to weld integrity (as can be seen in the tensile data reported in Table 3). Ideally, weld conditions should be sought which lead to a minimised defect length, allowing it to be easily machined off after welding is complete. This will be considered in more detail in the discussion in Section 3.3 and in Table 2, but the key controlling parameter appears to be downward forging force on the tool. Displaced metal from the tool and plate become entrained during rotation of the stud in the interfacial mixing zone (MZ), although the decrease in the forging force towards the top of the hole, due to the fact that the stud diameter is almost 1 mm less than the hole

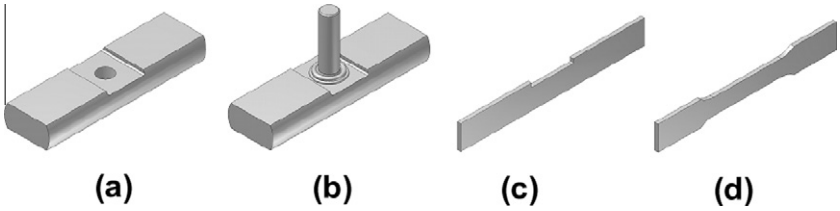

Fig. 4. (a) Sample before welding. (b) Completed weld. (c) Slice machined through the centre of the weld. (d) Final tensile hourglass specimen.

Table 3
Reduced experimental matrix using the Taguchi method.

Test equivalent	Tool speed	Downwards force	Plunge depth	UTS			
				Test 1 (MPa)	Test 2 (MPa)	Test 3 (MPa)	Average (MPa)
P19	*L*	*L*	*L*	420[a]	414[a]	252[a]	362
P23	*L*	*M*	*M*	–	474[b]	471[b]	473
P27	*L*	*H*	*H*	596[b]	–	341[b]	469
P13	*M*	*L*	*M*	883[d]	813[c]	533[a]	743
P17	*M*	*M*	*H*	741[b]	808[c]	892[b]	814
P12	*M*	*H*	*L*	178[b]	322[a]	276[c]	259
P7	*H*	*L*	*H*	–	869[a]	921[d]	895
P2	*H*	*M*	*L*	768[b]	–	531[b]	650
P6	*H*	*H*	*M*	558[b]	266[b]	226[b]	350

[a] Failure positions: along stud/hole interface.
[b] Failure positions: from flash crack defect.
[c] Failure positions: through weld.
[d] Failure positions: outside of HAZ.

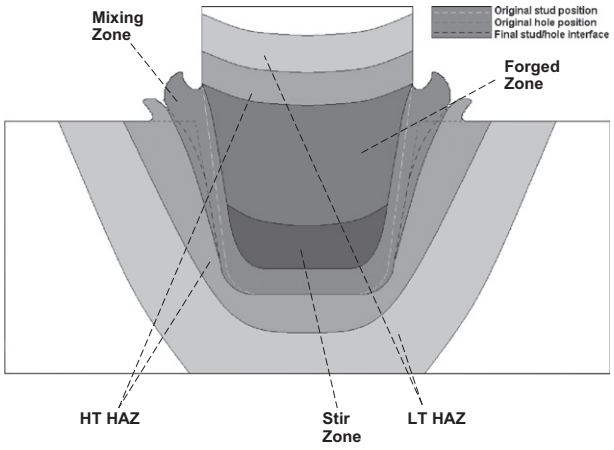

Fig. 5b. Different zones of a FTSW with the original stud and hole positions shown along with the final stud/hole interface.

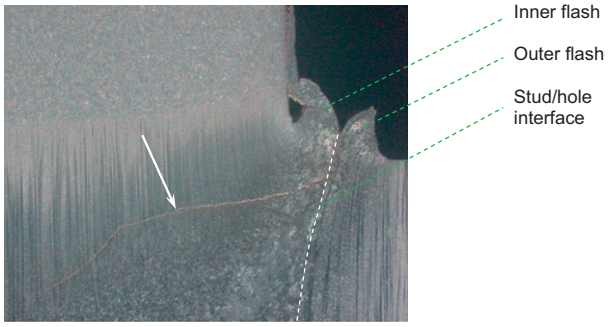

Fig. 6. Inner and outer flash streams which lead to an associated flash crack which initially runs down the stud–hole interface.

opening diameter at the surface, leads to incomplete mixing and the formation of the flash crack at the interface between the two streams of plasticised metal. Such defects follow the interface between the two streams of plasticised material for a short distance before veering off at an angle of some 45° towards the centre of the weld during cooling and contraction of the metal from peak temperatures close to 1000 °C (indicated with the white arrow in Fig. 6). The angle of this crack is affected by the forging or downwards force during welding, which will influence peak temperatures, their position and gradient near the surface of the plate. Above the heavily deformed stir zone (SZ) at the bottom of the weld is a region (FZ) in the interior of the stud where the major factor affecting deformation is the downwards forging force. In common with other welding techniques both high temperature (HTHAZ) and low temperature HAZ (LTHAZ) regions can be identified [12].

Hardness values were measured using a Vickers diamond indenter under a 500 gf load and representative values from three positions are given in Table 2. The weld zone hardness values appear to be related to the length of time taken to complete a weld (i.e. to the applied downwards force) and the tensile strength data given later in the paper (Fig. 10) indicate that the three combinations of process parameters that give the highest values of weld tensile strength also correspond with lower hardness values in the weld zone.

3.2. Torque and temperature data

Fig. 7 shows typical torque curves obtained in making four of the FTS welds. The caption gives the values for each weld of the

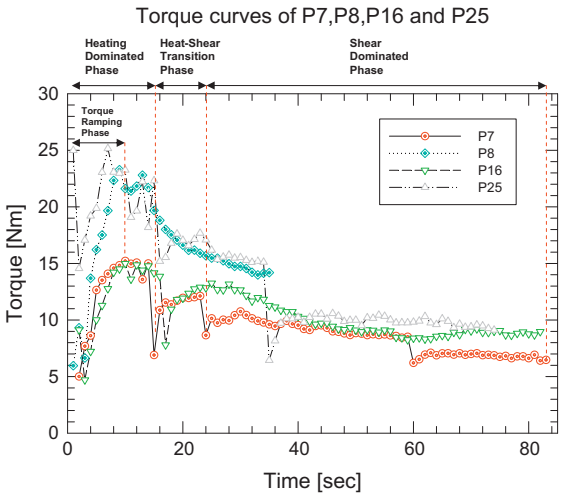

Fig. 7. Torsional response of samples P7 (*H L H*), P8 (*H M H*), P16 (*M L H*) and P25 (*L L H*).

three variable parameters of tool rotational speed, downwards force and plunge depth are indicated in that order, by upper case letters in brackets after the test identification characters. The tests shown are P25 (*L L H),* P16 (*M* L H), P7 (*H* L H) and P8 (*H* M H). Tests P25, P16 and P7 maintain a low value of applied force and a high value of plunge depth whilst increasing the tool speed from *L–M–H*. Tests P7 and P8 maintain a high tool speed and high plunge depth whilst increasing the downwards force from *L–M*. Fig. 7 indicates that the low tool speed in test P25 leads to a much higher initial torque value of around 25 Nm, compared with either test P16 or P7. This initially high value decays down to a similar value to that seen in tests P16 and P25 within 36 s. Thus in the 'steady-state' shear dominated phase of the welding tool rotational speed does not greatly influence the torque. These results agree with the results of other workers; e.g. Duffin and Bahrani [13] who observed that low rotational speeds produced excessive torque values in friction welding of mild steel. Medium (P16) and high (P7) tool speeds, in contrast, give self-similar torque curves over the whole welding period with lower peak values during the heating phase of around 15 Nm. Pinheiro [9] reports that work done in two studies by German authors also observed a higher torque peak as the rotational speed decreased in friction stir welding.

Fig. 7 indicates that high initial torque values do not necessarily coincide with shorter weld cycle times, and the key factor controlling weld cycle time appears to be forging force. Thus an approximate doubling in forging force from about 11 kN (P7, P16, P25) to some 21 kN (P8), leads to higher torque values during the initial heating dominated phase of the welding but also produces a weld in approximately half the time (35 s) compared with the low forging force (some 74–83 s). This decrease in welding cycle time with increase in downwards forging force is in agreement with the results of a number of studies reported by Pinheiro [9] covering steel and magnesium alloys and therefore appears to be a general conclusion irrespective of the alloy being welded. In terms of weld process optimisation, it would be clearly beneficial if process conditions could be identified that give similar mechanical properties with a shorter process time and the results contained in this paper represent a start point for this exercise.

Tensile data is considered in some detail in the next section, but it is worth noting that the test P7 (*H L H*) gave the highest measured value of tensile strength (an average of 895 MPa from two tests, equivalent to some 92% of the parent plate tensile strength). This is in contrast to the statement by Pinheiro [9] that improvement in weld quality is achieved by using lower rotational speeds.

It is, however, interesting to note that several combinations of process parameters give broadly similar average tensile strengths, although with significant specimen-to-specimen variability and that the particular combination of parameters used for test P8 were not identified as key by a Taguchi analysis. These observations highlight the difficulty in identifying routes towards process optimisation from a single parameter, such as torque, and consideration of multi-parameter surfaces is necessary.

Another important observation is that three main phases can be deduced from the torque data, which can be described as "heating dominated", "heat–shear transition" and "shear dominated" phases, as indicated in Fig. 7. The heating dominated phase can be defined as the time between the start of the weld and the point where substantial plastic shear occurs, which results in a substantial drop in peak torque. For sample P7 this phase ended at $t \approx 15$ s with the peak torque dropping from about 15 Nm–7 Nm. This point also corresponds with the attainment of the peak temperature recorded at the bottom of the sample, as indicated for sample P7 in Fig. 8. The torque then stabilises at a considerably lower plateau level for the remainder of the weld, indicating a changeover from the heat–shear transition phase to the shear dominated phase. For sample P7 this happened at about 24 s. An additional torque ramp-up stage occurred within the first 10 s of welding, during which the maximum process torque was recorded. This phenomenon can be related to overcoming friction at start-up when the work piece is still relatively cold. Similar torque characteristics in friction welding of round bars were reported by Hasui and Fukashima who did studies on medium and high carbon steels [14].

It was suggested in some early work on friction welding that the duration of this initial heating dominated phase should be one of the fundamental parameters used to control the friction welding process [15]. Pinheiro [9] gives a useful summary of a number of studies which have reported observations of the duration of the heating time and the role of temperature in the weld process. The view of the present authors is that process-property generalisations drawn from observations of heating time should be treated with caution. For instance, Pinheiro [9] reports results from five studies which indicated that the heating time increased with increasing rotational speed. This is not supported for the present technique and alloy by the results of tests P7, P16 and P25 where the heating time appears to be almost constant over a significant range of speed, from 2500 rpm to 6000 rpm.

Pinheiro [9] himself highlights a difficulty in interpreting weld temperature–time relationships in terms of weld performance. He notes that to obtain an improvement in weld 'quality' (which is not clearly defined by him) it is normally desirable to have short heating times, but that when it is desirable to preserve toughness or have lower hardness, longer heating times and lower cooling rates are beneficial. FTSW introduces an additional complexity in interpreting weld properties from temperature data is as indicated in Fig. 8.

Typical temperature data obtained with thermocouples at three positions in the weld are given in Fig. 8 for specimen P7 (*H L H*) as a function of time and plunge depth. The bottom of the weld reaches an almost steady-state temperature within 20 s of the start of the welding process and stabilises at a temperature of between 650 °C and 750 °C, whilst the temperature at the middle and top of the weld continue to increase throughout the weld duration. The rate of tool consumption (plunge depth) initially slows down but then accelerates towards the end of rotation as the interfacial stud material reaches higher temperatures. Although the recorded axial displacement shows a maximum plunge depth of only 8 mm, measuring the completed weld shows that the actual total plunge depth reached 9 mm. Once rotation is halted, the axial downwards force is maintained for 20 s to consolidate the weld which likely causes an additional nominal amount of tool displacement due to compression of the hot plasticised material.

3.3. Tensile strength

In order to focus on the key combinations of process variables that would achieve optimum welding in terms of tensile strength, the Taguchi method of experiment design was used. This is a standardised statistical approach which can reduce the number of tests required to explore relationships amongst a given set of variables and their values [16]. Use of the method reduced the required number of tensile tests from 27 to 9. Table 3 gives the reduced matrix of nine combinations of process parameters together with the resultant tensile strengths and the position in the specimen where failure occurred. In the highest strength weld failure occurred away from the weld zone and demonstrates that FTSW can reach tensile strengths of some 94% of the parent plate strength (921 MPa).

Fig. 9a–c presents contour surfaces of tensile strength as a function of combinations of the three process variables, plunge depth, tool rotational speed and downwards force which are used to ascertain trends between the input parameters and the tensile data. Fig. 9a indicates that there is a substantial range of combinations of rotational speed and downwards forging force that lead to high tensile strength. Test P7 with high speeds (6000 rpm) with low forging force (≈11 kN) and test P17 with medium speeds (4250 rpm) and medium forging force (≈21 kN) give the highest average values of weld tensile strength of 895 MPa and 814 MPa

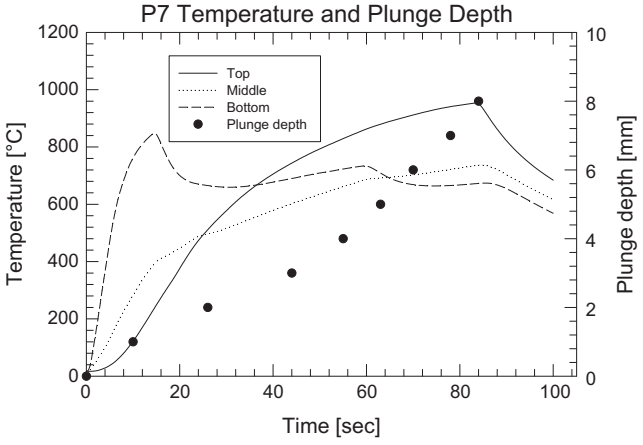

Fig. 8. Temperature responses of top, middle and bottom thermocouples with superimposed plunge depth rate of process test sample P7.

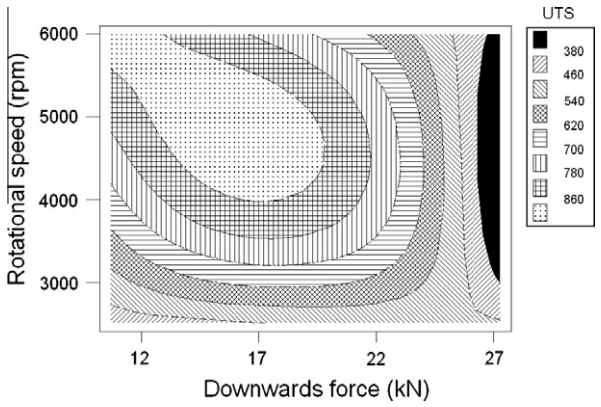

Fig. 9a. The effect of rotational speed and downwards force on tensile strength.

respectively. Forging force and plunge depth (Fig. 9b) are somewhat inter-related parameters and have a narrow band where optimum tensile strength occurs. The welding machine used for this work did not have the power to fully explore this region, and for the experimental matrix used, the highest value of plunge depth (≈8 mm) is required with low to medium forging force (tests P7 and P17). Fig. 9c plots plunge depth against tool rotational speed. The highest average value of tensile data is again found in a narrow range of high plunge depth and high tool speed (test P7).

The trends in these contour maps can be presented more clearly as shown in Fig. 10, by plotting the average value of tensile strength for each combination of parameters used in the Taguchi analysis. This average tensile strength varies in a systematic way from 259 MPa to 895 MPa. The combination of parameters (*H L H*) giving the highest average value also gave the peak measured tensile strength value of 921 MPa (94% of the parent plate value). The ranking of tensile strength as a function of process parameters is interesting, leading to the interpretation that tool rotational speed is less important than forging force or plunge depth. This can be discerned as medium and high speeds are associated with the lowest strength welds and with the highest strength welds. A high forging force with a low plunge depth (P12) provides the lowest strength weld (259 MPa). In terms of average value of tensile strength, there is little to choose between tests P6 (350 MPa) and P19 362 MPa). Tests P23 (472 MPa) and P27 (469 MPa) are also close together and then the tensile strength data steadily improves in order through tests P2 (650 MPa), P13 (743 MPa), P17 (814 MPa) and P7 (895 MPa).

Thus the present study of FTSW of high strength steel indicates a general trend towards stronger welds for combinations of medium to high rotational speed with medium to low forging force,

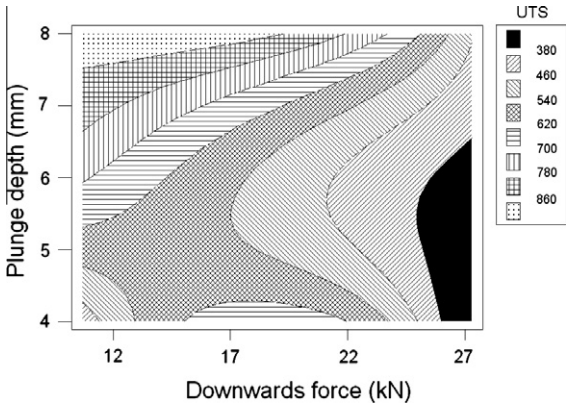

Fig. 9b. The effect of plunge depth and downwards force on tensile strength.

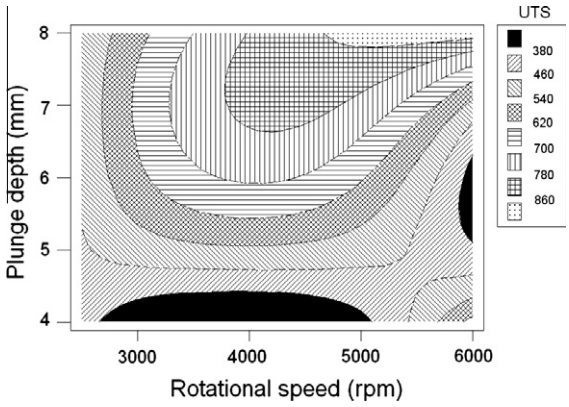

Fig. 9c. The effect of plunge depth and rotational speed on tensile strength.

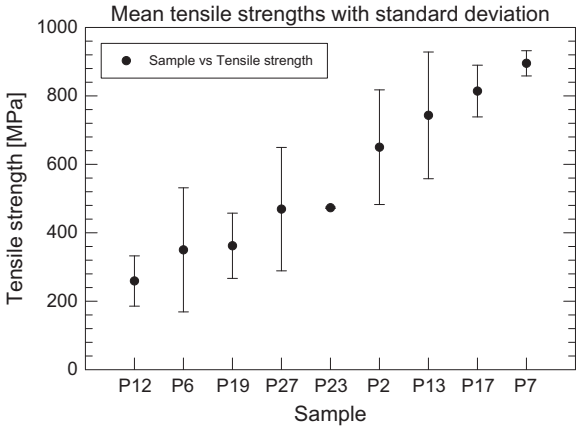

Sample	P12	P6	P19	P27	P23	P2	P13	P17	P7
RPM	M	H	L	L	L	H	M	M	H
DOWNWARDS FORCE	H	H	L	H	M	M	L	M	L
PLUNGE DEPTH	L	M	L	H	M	L	M	H	H

Fig. 10. Tensile strengths as a function of different parameter combinations.

and that the tensile strength then tends to increase as plunge depth increases.

In contrast to these results, Pinheiro [9] found, in his study on FHPP of low strength magnesium casting alloys that increasing the welding pressure increased the tensile strength of the welds. The relationship between tensile strength of the bond and the forging force appears to be influenced by the degree of consolidation of the lower part of the weld [17] that occurs before the upper part of the weld is completed. This is very likely to be strongly affected by taper angle of the weld hole and tool, and by the alloy and its high temperature plastic deformation response.

A further important factor influencing tensile strength is the occurrence and type of weld defects, the most prominent being the flash crack defect mentioned earlier. Their occurrence is linked with the magnitude of the downward force during welding, and at low values of this force such defects are either absent or are consistently shorter than is found at higher force values. This can be clearly seen in the data given in Table 2. Other internal defects, apparently induced by shear processes, occur in the weld region but do not appear to have a significant influence on tensile strength. Fig. 11 shows the polished cross-section of the weld P7 (*H* L H) which, despite the existence of these shear-induced defects, still exhibited the highest average tensile strength.

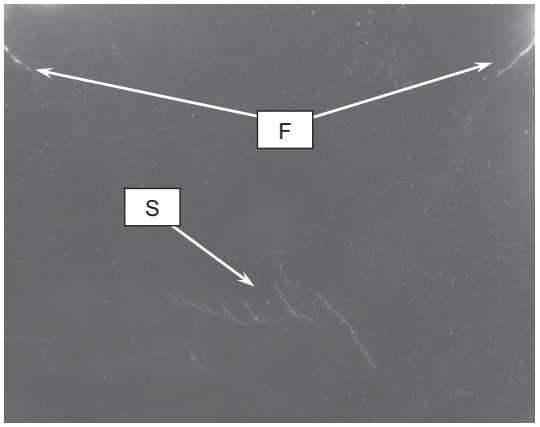

Fig. 11. Polished surface of process test sample P7 showing internal shear (*S*) and flash crack (*F*) defects.

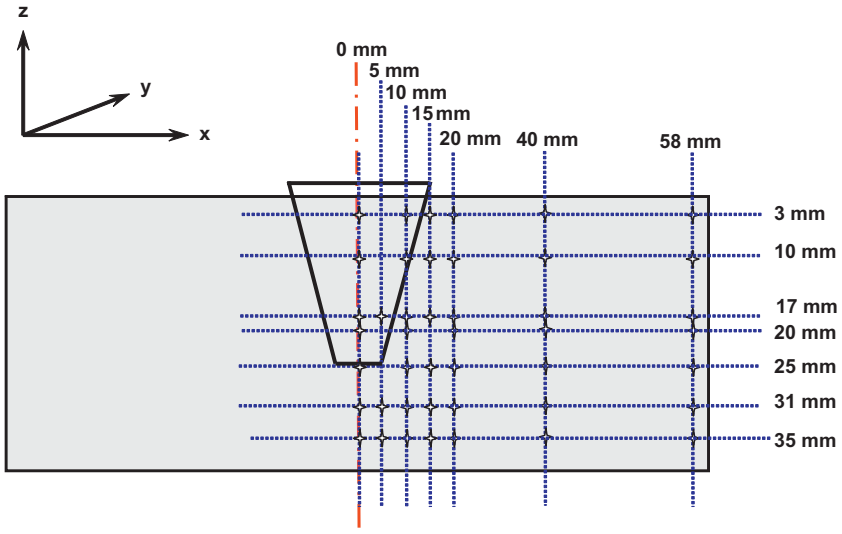

Fig. 12a. Matrix of points at which residual stresses were measured for a FTSW in 10CrMo910 steel using neutron diffraction strain scanning. The axis directions are indicated in the image.

3.4. Residual stresses

Residual stress distributions and their modification during service are highly influential factors on performance of welded joints. This particularly true in the case of stress corrosion cracking which is often found in steam nozzles and piping [18], or where they can add to imposed service stresses and enhance creep damage accumulation. With this in mind, residual stress profiles in typical FTS welds have been extensively characterised for the 10 CrMo 9 10 steel mentioned earlier in the paper, using neutron diffraction strain scanning. This work was performed at the Institute Laue–Langevin on the SALSA instrument (experiments 1-01-08 and 1-01-58) on as-welded and on heat treated samples. Additional strain scanning on overlapping 13 CrMo 44 FTS welds has been conducted at the Rutherford Appleton Laboratory, ISIS-ENGIN-X (experiment RB720574). Some of this work has been reported elsewhere [19].

In view of the importance of residual stresses in relation to service performance and their dependence on weld process parameters, it is useful to present typical 3D residual stress data

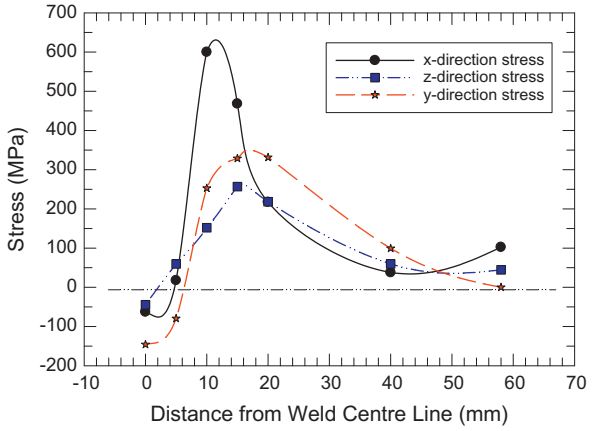

Fig. 12b. Residual stress data in the three coordinate directions, measured along the points on the line 10 mm below the surface of the FTSW weld in 10CrMo910 steel.

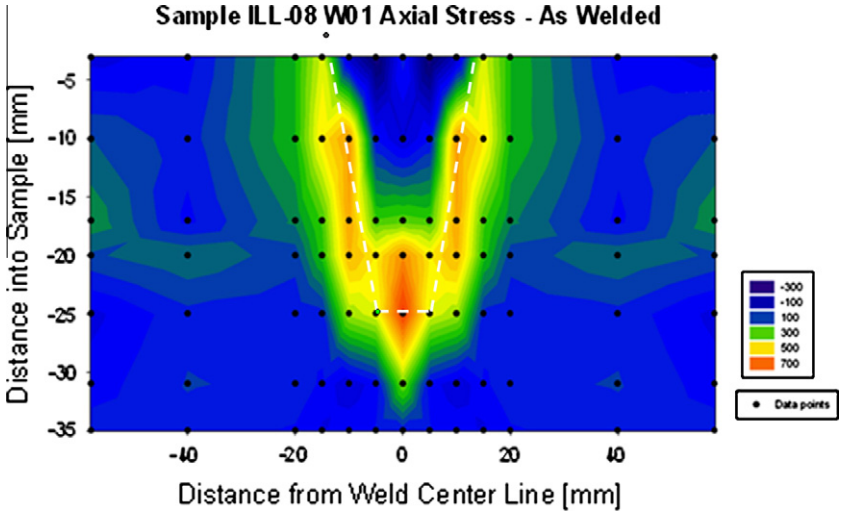

Fig. 12c. Map of the *x*-direction residual stress data for a FTSW weld in 10CrMo910 steel.

in any paper dealing with novel welding processes. The distribution of residual stresses would be expected to be similar in 4140 and 10 CrMo 910 steel although peak values may be higher in the 4140 steel. Figs. 12b and 12c present as-welded 3D residual stress data measured at the coordinate intersection points shown in Fig. 12a for a FTSW made in 10 CrMo 910 alloy. It can be seen that the peak tensile values of residual stress occur close to the position of the original hole boundary (i.e. in the mixing zone in Fig. 5b). The overall form of the residual stress distributions in all three coordinate directions is similar with tensile residual stress values occurring in the mixing zone and peak values observed at the bottom of the weld. This form of distribution reflects the particular temperature distribution that occurs during friction taper stud welding and would be expected to be very similar in the case of 4140 steel.

The relatively high residual stresses shown in the as-welded condition (Fig. 12c) correlate well with the presence of internal defects observed in the stir zone (Fig. 11). Cracking would be promoted by tensile residual stresses aided by precipitate segregation at the grain boundaries. This observation highlights the importance of pre- and post-weld heat treatment in steels with high carbon equivalent values such as AISI 4140 and 10 CrMo 910 alloys.

4. Conclusions

This fairly comprehensive study of the influence on tensile strength and defects of three key process parameters in FTSW, namely tool rotational speed, forging force and tool plunge depth, allows the following conclusions to be drawn regarding this useful development of FHPP:

(1) Metallographically, the weld zone and surrounding regions display several distinct regions during FTS welding that have been identified in Figs. 5a and b as a stir zone (SZ), mixing zone (MZ), forged zone (FZ), high temperature heat affected zone (HT HAZ) and low temperature heat affected zone (LT HAZ).
(2) The time taken to complete the weld can be related to energy input and forging force. In this high strength 4140 steel alloy the heating time to peak temperature in the welding cycle does not appear to vary much over the chosen range of process conditions.
(3) Weld cycle time reduces as the forging force increases. Results of other workers using different alloys support this [9] and this therefore appears to be generally true.
(4) The torque input during welding for the parameter combination (high rotational speed, low downwards force and high plunge depth) which produced the weld with the highest tensile strength can be divided into heating dominated, heat–shear transition and shear dominated phases. These phases are less distinguishable in welds with lower rotational speeds and higher downwards forces.
(5) Low downwards force, high rotational speed and high plunge depth not only produce the highest average tensile strengths, but also give a relatively low standard deviation in tensile strength of about 37 MPa. In contrast, high downwards forces produce low tensile strengths with high specimen-to-specimen variation as seen with samples P12, P6 and P27.
(6) The relationship between tensile strength of the bond and the forging force appears to be influenced by the degree of consolidation of the lower part of the weld that occurs before the upper part of the weld is completed. This is very likely to be strongly affected by taper angle of the weld hole and tool, and by the alloy and its high temperature plastic deformation response.
(7) A maximum tensile strength of 94% of the parent material was achieved with a (*H* L H) combination of process parameters.
(8) Two major types of defects were observed, flash cracks at the interface between the two streams of plasticised metal and internal shear cracks in the stir zone. The most influential defect is the flash crack which can lead to much lower tensile strengths.

Acknowledgements

The authors gratefully acknowledge the award of beam-time on the SALSA instrument at the Institut Laue–Langevin in Grenoble (experiments 1-01-08 and 1-01-58) and assistance from the beamline scientist, Dr. D. Hughes. The residual stress data shown in Fig. 1 was computed from data obtained during experiment 1-01-58 with the assistance of Prof. A. Steuwer, Mr. P. Doubell and Mr. M. Newby.

References

[1] Nonaka I. Residual life evaluation and repair procedures for high temperature boiler piping. Oper, Maint Mater Iss 2003;2(1):1–14. <http://www.ommi.co.uk>. [accessed 22.11.10].
[2] Abbasi W, Rahman S, Metala MJ. NDE and material evaluation for lifetime assessment of power plant components. In: Proceedings of the tenth European conference on non-destructive testing, Moscow; 7–11 June, 2010. Paper 4_01_09, <http://www.ndt.net/article/ecndt2010/reports/4_01_09.pdf>, [accessed 22.11.10].
[3] Ambroziak A, Gul B. Investigations of underwater FHPP for welding steel overlap joints. Arch Civil Mech Eng 2007;7(2):67–76.
[4] TWI. Leading edge. Friction hydro pillar processing. Connect; June 1992.
[5] Hattingh DG, Newby M, Steuwer A, Wedderburn IN, Doubell P, James MN. Friction taper stud welding of creep resistant 10CrMo910 steel. TMS Frict Stir Weld Process-V 2009:75–84.
[6] Thomas W, Nicholas D. The need for gas shielding – positive advantages for two friction processes. TWI Bull 1997(September/October):84–8.
[7] Andrews RE, Mitchell JS. Underwater repair by friction stitch welding. Met Mater – Mar Technol 1990(December):796–7.
[8] Thomas WM, Nicholas ED. Emerging friction joining technology for stainless steel and aluminium applications. TWI, productivity beyond 2000: IIW Asian Pacific Welding Congress, Auckland, New Zealand; February, 1996.
[9] Pinheiro GA. Local reinforcement of magnesium components by friction processing: determination of bonding mechanisms and assessment of joint properties. GKSS Report 2008/12, Geesthacht; 2008. ISSN 0344-9629.
[10] Van Zyl CAA. Analysis and modelling of the temperature distribution during the friction taper stud welding of 10CrMo910. Masters Dissertation, Nelson Mandela Metropolitan University; 2008.
[11] ASTM Standard E8M-01. Standard test methods for tension testing of metallic materials (Metric). West Conshohocken, PA: ASTM International; 2002.
[12] Du Toit M, Van Rooyen GT, Smith. An overview of the heat-affected zone sensitization and stress corrosion cracking behaviour of 12% chromium type 1.4003 ferritic stainless steel. Paper presented to the Southern African Institute of Welding 60th Anniversary Conference, Gold Reef City South Africa; 28–29 May, 2008. p. 16.
[13] Duffin FD, Bahrani AS. Friction welding of mild steel. Met Constr Brit Weld J 1973;05(04):125–32.
[14] Hasui A, Fukashima S. On the torque in friction welding. J Jpn Weld Soc (in Japanese) 1975;44(12):1005–10.
[15] Vill VI. Friction welding of metals. New York: Reinhold Publishing Corporation, American Welding Society; 1962.
[16] Roy RK. A primer on the Taguchi method. The United States, Van: Nostrand, Reinhold; 1990.
[17] Meyer A. Friction hydro-pillar processing – bonding mechanism and properties. Fakultät für Maschinenbau und Eletrotechnik der Technischen Universität Carolo-Wilhelmina zu Braunschweig; 2003.
[18] Okimura K, Mukai M, Kamo K, Hori N, Masumoto K, Kurokawa M. Maintenance strategies for SCC which support stable operations of pressurised water reactor power plants, Mitsubishi heavy industries ltd.. Tech Rev 2006;43(4):1–5.
[19] Hattingh DG, Steuwer A, James MN, Wedderburn IN. Residual stresses in overlapping friction taper stud welds. In: Proceedings of MECA-SENS 5, fifth international conference on mechanical stress evaluation by neutrons and synchrotron radiation, Mito, Japan, 10–12 November, 2009, Materials Science Forum, vol. 652; 2010. p. 111–5.